UNIVERSITYOF BIRMINGHAM

Ti-Fe Phase Evolution and Equilibria Toward β-Ti Superalloys

O'kelly, P.; Watson, A.; Schmidt, G.; Galetz, M.; Knowles, A. j.

[Link to publication on Research at Birmingham portal](#)

ORIGINAL RESEARCH ARTICLE

Ti-Fe Phase Evolution and Equilibria Toward β-Ti Superalloys

P. O'Kelly[1] · A. Watson[1,2] · G. Schmidt[3] · M. Galetz[3] · A. J. Knowles[1]

Abstract Recent design and development of precipitate reinforced refractory metal alloys demonstrate the possibility of A2 + B2 bcc superalloys as a new class of high temperature materials. Existing β-Ti alloys do not typically employ reinforcement with intermetallics, as in other high temperature alloys; to this effect sufficient additions of Fe, a low cost β-Ti stabiliser, can promote formation of an ordered-bcc intermetallic phase, β′-TiFe (B2), offering scope to develop a β + β′ dual-phase field. However, key uncertainties exist in the base Ti-Fe binary. The current research evaluates the formation of ordered-bcc TiFe precipitates within a disordered-bcc β-Ti matrix through variable heat treatment strategies. The microstructure optimisation has revealed new insight into the Ti-Fe phase equilibria at near eutectoid temperatures in the purported dual-phase field, where a complex interplay between β-Ti, β′-TiFe and α-Ti exists.

Keywords bcc-superalloy · evolution · equilibria · phase · Ti · Ti-Fe

✉ A. J. Knowles
a.j.knowles@bham.ac.uk

1   Present Address: School of Metallurgy and Materials, University of Birmingham, Birmingham, UK

2   Hampton Thermodynamics Limited, Hampton, UK

3   DECHEMA-Forschungsinstitut, Frankfurt am Main, Germany

1 Introduction

Efforts to extend the capabilities of Ni-based superalloys have been ongoing for over six decades. The economic and societal benefits are vast—the ability to increase gas turbine operating temperature results in improved efficiency and reduces emissions, two priorities of 21st century aviation. Twenty-five years ago, an effort to develop bcc superalloys began, starting from B2-NiAl. Through additions of disordered bcc (A2) transition metal elements, A2 + B2 microstructures were achieved[1] in the multi-component systems X-Ni-Al (@ X = Fe, Cr, V) within a certain composition range. Substituting some Al for Ti produced a microstructure of cuboidal L2$_1$ precipitating from a disordered bcc matrix, analogous to the γ-γ′ found in nickel-superalloys. The strategy of incorporating ordered aluminide phases (B2 or L2$_1$) was also extended to development of Nb-based superalloys[2] where precipitation of B2-PdAl, L2$_1$-Pd$_2$HfAl or Ru$_2$NbAl ordered phases were investigated.

Intense work on Refractory High Entropy Alloys (RHEA) and Refractory Complex Concentrated Alloys (RCCA) dominated since the late 2000's and 2010's resulting in A2+B2 microstructures reminiscent of FCC γ-γ′ microstructures: a high-volume fraction of coherent ordered precipitates in a disordered matrix phase. Thus, a renewed effort is underway to further develop the early work of Naka and Khan[1] and understand Ti-Al-X (@ X = Cr, Fe, Mo, Nb, Ta, V, W) systems, particularly the role Al plays in B2 formation in these ternary and higher order systems.[3–5]

The Ti-Fe system is an interesting base system upon which to investigate a concept 'bcc-superalloy' for high temperature capability. The β-Ti phase offers significant density improvements over high temperature alloys based

J. Phase Equilib. Diffus. (2023) 44:738–750

739

on Ni, Fe and Co, while for structural applications the high specific strength of titanium alloys is well documented. Additionally, Fe is a potent and low cost β-Ti stabiliser. Recent work has utilised ordered-bcc-TiFe (B2) as an alternative to ordered aluminides as the reinforcing phase,[6] thus scope exists to exploit dual phase β-Ti + β′-TiFe phase field by analogy to nickel-based superalloys based on Ni-Al. However, the binary systems are themselves not always fully understood. For example, the additions of Fe, required to promote formation of the ordered-bcc TiFe (B2) phase within β-Ti (A2). A recent study[7] targeting the A2 + B2 dual phase field also reported the presence of minor phase fractions of the hcp α-Ti phase. Furthermore, Ti-X binary systems containing eutectoid formers and isomorphous solutes also display complex mechanisms regarding their evolution of secondary phases and the products of decomposition of the β-phase, for example in active eutectoid systems (e.g. Ti-Cu[8]) and systems exhibiting spinodal decomposition.[9] These present significant complexities in stabilising the β-Ti phase, across the many potential β-stabilising elements.

Additionally, it is worth noting interest in the Ti-Fe system in the context of sustainable energy. TiFe is a promising low-cost hydrogen storage material, though challenges persist regarding its activation.[10]

The solid solution equilibrium phases of the Ti-Fe system consist of the following.[11] The hexagonal and cubic polymorphs of the pure-Ti phase: the hexagonal polymorph (A3) is stable below 882 °C while the body-centred cubic (A2) titanium is the high temperature phase above 882 °C. Pure Fe (α-Fe, A2) is also body centred cubic stable below 911 °C and above 1392 °C. The face centred cubic γ-Fe (A1) solid solution is stable between 911 and 1392 °C. The two equilibrium intermetallic phases in the binary system are the equiatomic TiFe and the $TiFe_2$ Laves phase. The TiFe is CsCl-cubic (B2) forming peritectically from the melt (L + C14 →TiFe) at 1317 °C. This phase is stable to room temperature with some compositional homogeneity. The $TiFe_2$ Laves phase (C14) has a hexagonal $MgZn_2$ structure and melts congruently at 1427 °C.

In all thermodynamic assessments of the Ti-Fe system, the experimental work of Van Thyne et al.[12] singularly informs the titanium rich region of the equilibrium phase diagram relating to the β-Ti transus gradients, eutectoid composition and eutectoid transformation temperature, which was determined to be 595 °C. In their work, iodide titanium was used to determine the constitution of titanium rich alloys up to the stoichiometric TiFe phase. No oxygen impurity of starting materials was reported, though minor impurities in the raw Fe product were given. A combination of x-ray diffraction, thermal analyses and microstructural observations using optical microscopy were used to deduce the phases present following heat treatments between 500 and 1200 °C, which informed their subsequent phase diagram. In later work[13] investigating hypo- and hyper-eutectoid alloys using powder metallurgy, to specifically address the contribution of contaminants on phase equilibria, the eutectoid temperature was found to be higher than that reported by VanThyne[12] at 625 ± 10 °C. A key finding was the presence of the Ti_2Fe phase (space group:$Fd\overline{3}m$) at 1000 °C in hypereutectoid alloys with oxygen contents in the range 0.5–1.0 at.%. This was considerably less than the minimum 2 at.% reported by others[14] and proposed the inclusion of Ti_2Fe as a stable binary phase, which was widely debated. An experimental re-evaluation of the Ti-Fe and Ti-Fe-O systems[15] investigated a range of alloys in the vicinity of the reported Ti_2Fe composition in the binary Ti-Fe and in the Ti-Fe-O system. The authors concluded, with post heat-treatment oxygen levels of approximately 0.1 at.%, that Ti_2Fe exists, forming peritectoidally from β + TiFe at around 1000 °C. Interestingly, they support their result by the observation that the Ti_2Fe structure, a complex fcc (strukturbericht $E9_3$) with cell side of 11.34 Å,[13] is observed in the systems Ti-Fe-Mo and Ti-Fe-V, Ti-Fe-Al, with oxygen contents that cannot correlate to the phase fraction of the disputed $Ti_2(Fe,X)$ present.

All the preceding experimental data to this point was critically assessed and a resulting Ti-Fe phase diagram was produced based on this bibliographic information.[16] The salient features of this phase diagram are the limited solubility of Fe in α-Ti, the off-stoichiometric composition range of the C14 Laves phase and the γ-Fe loop. There are two recent experimental investigations examining characteristics of the Ti-rich region of the binary system. One is a brief examination of phases present at 600 °C in Ti-20Fe (at.%) alloy,[7] where the presence of α-Ti is reported in the supposed dual A2 + B2 phase field. The second experimental work[17] utilises diffusion couples to determine interaction mobility parameters of Ti and Fe in the disordered-bcc phase at 900 °C and 1000 °C. These parameters were optimised within the Thermo-Calc module DICTRA to compare modelled diffusion profiles with experimental profiles obtained by EPMA.

An early CALPHAD style assessment of the Ti-Fe system was given by Kaufman and Nesor.[18] Following the critical assessment of the binary phase diagram by Murray,[16] a succession of thermodynamic assessments and re-assessments were made in the decade after, which were compared by Dumitrescu and Hillert[19] who note the difficulty in fitting all of the phase diagram information coherently, specifically relating to the reproduction of the eutectoid composition of bcc in equilibrium with ordered bcc TiFe and the hexagonal α-Ti phase, also discussed in previous assessments by Kumar et al.[20] and Jonsson.[21]

The main points of difference in each of the thermodynamic assessments (with respect to the composition space hcp Ti to stoichiometric TiFe) concern new data on specific heat capacity of the TiFe and TiFe$_2$ intermetallic phases, which informs the phase diagram of Dumitrescu and Hillert.[19] Additionally, there is variation in the location of the eutectoid composition (12–15 at.% Fe) and temperature (565–595 °C) by each author which leads to the conclusion by Dumitrescu and Hillert that a new thermodynamic assessment should not be attempted until further experimental work is performed.

The works of Dumitrescu and Hillert,[19] Kumar et al.[20] and, later, Ohtani et al.[22] all represent the stoichiometry of the TiFe phase as a line compound. This practice is common when approximating phases with a limited homogeneity range to simplify the calculation. However, Murray[16] projects a homogeneity range of TiFe of 49.7 to 52.5 at.% Ti based on a revised experimental evaluation of the binary system from the initial publication. Interestingly, in work investigating the order-disorder transition in Ti-Fe alloys from 10 to 50 at.% Fe by splat quenching,[23] single phase CsCl (B2) structure was retained in alloys with compositions 37.5–50 at.% Fe.

The many assessments of the binary system have been incorporated in higher order descriptions sporadically. The initial CALPHAD style assessment by Kaufman and Nesor[18] was used to predict isothermal sections of ternary systems Ti-Fe-Mn and Ti-Fe-Al systems,[24] which served as comparison to experimental observations to test the viability of the CALPHAD technique. More recently, the Ti-Fe-Cr[25] and Ti-Fe-V[26] systems have been modelled based on the Ti-Fe binary thermodynamic data. Both works rely on the assessments compared by Dumitrescu and Hillert,[19] which is to say at the time of writing there has been no further experimental investigation of the eutectoid composition or temperature as recommended in the review.

1.1 Experimental Procedure

In order to investigate the phase equilibria in the Ti-Fe system, two alloys were prepared, with compositions Ti-4.3Fe and Ti-22Fe (at.% used hereafter), which are shown superimposed on the equilibrium phase diagram in Fig. 1. These were selected to investigate the respective β-transus gradients. Additionally, the Ti-22Fe alloy lies in the β-Ti + β′-TiFe (A2-B2) two-phase field over a wide temperature range. This enabled investigation of the phase equilibria as a function of temperature and to probe the nucleation characteristics of the B2-TiFe intermetallic.

The alloys Ti-4.3Fe and Ti-22Fe (Ti purity > 99.9%, Fe purity > 99.95%) were manufactured by vacuum arc button melting on a water-cooled copper hearth under high purity Argon by TIMET UK. Bulk composition analysis of the as-manufactured alloys was determined by x-ray Fluorescence (XRF) analysis by TIMET UK. The oxygen content in their as-manufactured condition was determined by LECO inert gas fusion.

From each of the as-cast ingots, sections were cut and wrapped in pure tantalum foil. These samples were put into a single quartz ampoule which was evacuated and backfilled with argon, encapsulated, and sealed. A homogenizing treatment of 1050 °C for 24 h followed by water

Fig. 1 Ti-Fe equilibrium phase diagram adapted from Murray.[16] Bulk alloy compositions investigated in this work are marked within red dotted lines.
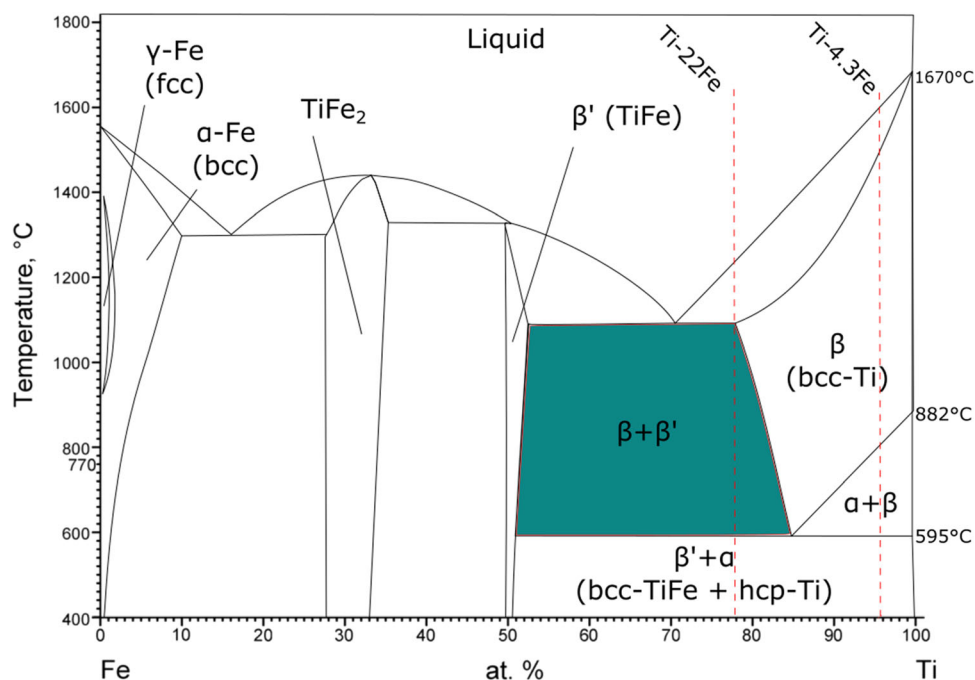
quench (WQ) was applied. Samples were cut from the homogenised bulk alloys for conventional ageing heat treatments, which were applied by inserting the argon backfilled ampoule into a furnace set at the ageing temperature. A K-type thermocouple was used to confirm the furnace temperature. All aged samples were water quenched.

X-ray diffraction (XRD) was carried out with a Proto AXRD diffractometer using Cu Kα radiation. Lattice parameters were determined using the Nelson-Riley method.[27] Lattice parameters of the β-Ti and β′-TiFe were calculated by estimating the lattice parameter associated with each peak, plotting against the Nelson-Riley parameter to determine the linear regression, and determining the y-intercept. The a and c parameters of α-Ti were calculated from $\{10\bar{1}0\}$ and $\{0002\}$ reflections and confirmed through higher order reflections.

Standard metallographic preparation techniques were used to prepare samples for microstructural characterisation. The microstructure was characterized in a JEOL 7000F FEG scanning electron microscope (SEM) operated at 20 kV, with compositions evaluated using energy dispersive spectroscopy (EDS) in the same SEM. Electron probe microanalysis (EPMA) was conducted using a JEOL JXA 8100 with a W cathode at an acceleration voltage of 15 kV and a probe current of 30 nA.

Transmission Electron Microscopy (TEM) foils were prepared using the Focused Ion Beam (FIB) process on a FEI-Quanta 3D FEG FIB SEM. TEM selected area diffraction patterns (SADP), bright field (BF) and dark field (DF) images were collected using a JEOL 2100 at 200 kV.

Scanning transmission electron microscopy (STEM)-EDS analyses were performed using a Philips Tecnai F20 at 200 kV.

2 Results and Discussion

Impurity levels in the as-cast ingots were determined by gas fusion method and are presented in Table 1. The oxygen levels are below typical impurity levels found in commercially produced titanium alloys, which are on the order of 1500 ppm.

The homogenised alloys exhibited intense peaks in the range 30°–90° 2θ, Fig. 2, indicating that the system consisted of β-phase only, with a lattice parameter a_β of 3.304 Å for Ti-4.3Fe and 3.151 Å for Ti-22Fe. The microstructure of each alloy is shown in Fig. 2(b) which revealed no minor phases, along with SEM-EDS line profiles which confirm the target bulk composition following homogenising heat treatment.

In order to determine the β/β + β′and β/β + α transus gradients, conventional ageing of previously homogenised bulk samples for 8 h was performed followed by rapid water quench. The ageing temperatures applied were 650, 675, 700, 725, 750, 800 and 900 °C. The matrix composition of each respective alloy was measured by SEM-EDS by averaging 10 Point & ID data-points, a summary of which is presented in Fig. 3. It is seen that the overall trend of the gradients does not deviate significantly from the accepted phase diagram[16] therefore the eutectoid temperature is considered to be in agreement.

During the determination of the β/ β + β′ transus gradient, for the Ti-22Fe alloy a three-phase microstructure was unexpectedly observed for all ageing temperatures.

Table 1 Impurity level (at.%) chemical analyses determined by gas fusion method from as-cast ingots

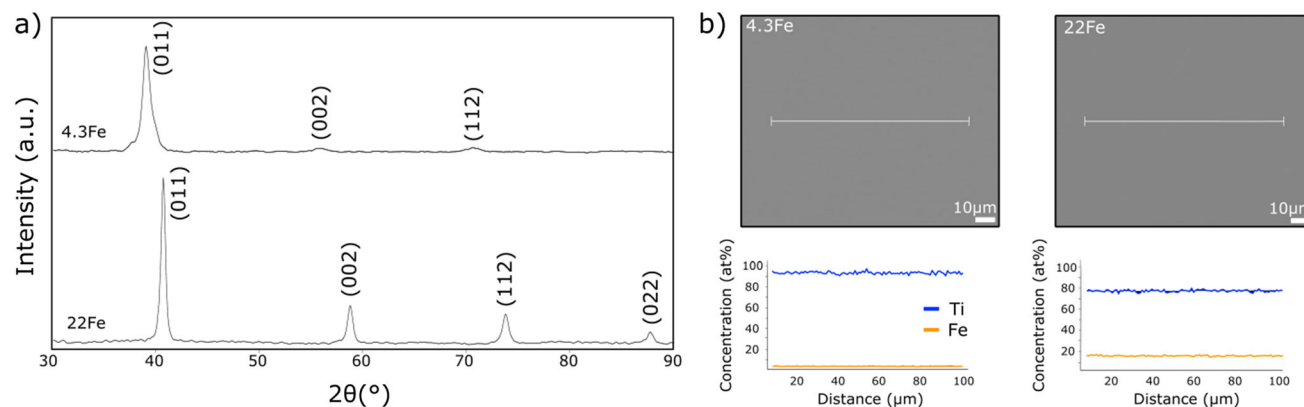| Fe	O	C, ppm	H, ppm	N, ppm
4.3	0.30	60	84	1049
22	0.05	30	32	1440

Fig. 2 (a) XRD spectra of the alloys homogenised at 1050 °C for 24 h showing single-phase A2 β-Ti reflections, (b) BSE micrographs and SEM-EDS profiles of the homogenised alloys show no microstructural features or composition variation

742

J. Phase Equilib. Diffus. (2023) 44:738–750

Figure 4(a) shows the XRD spectra for the alloy aged at 650 and 800 °C where, in addition to expected primary β-Ti(-Fe) and superlattice β′-TiFe peaks, additional peaks are also observed. These additional peaks were consistently attributable to the α-Ti phase (*space group* P6₃/mmc) up to 725 °C, while from 725 to 900 °C the additional peaks were consistent with the Ti₂Fe phase (*space group* $Fd\bar{3}m$),

reportedly a complex fcc structure (*Strukturbericht* $E9_3$).[13]

Representative microstructures of the Ti-22Fe alloy following ageing at 650 °C and 800 °C are shown in Fig. 4(b) and (c), where TiFe precipitates are homogeneously distributed in the grain interior. However, the non-equilibrium state at 650 °C is suggested by "floret" morphologies, seen in the higher magnification BSE-SEM micrograph highlighted in Fig. 4(b), where the fine scale lamellae with dark contrast (indicated) are the α-Ti peaks observed in the XRD spectrum in (a). Owing to the length-scale of the floret, composition analyses using SEM-EDS point identification was not possible. In the absence of unidentified peaks in the XRD spectrum, in addition to BSE-contrast images, it is assumed that β′-TiFe is the remaining constituent of this morphology. Fig.4(c) is the representative microstructure obtained from ageing at 800 °C for 8 h followed by water quench. In addition to the discrete β′-TiFe precipitates, larger coarse laths are also observed. SEM-EDS analyses indicate the composition of these laths is approximately that of Ti₂Fe, which is not an equilibrium phase according to the accepted phase diagram.[16] The respective phases in equilibrium at 650 °C are (β + β′ + α), and at 800 °C are (β + β′ + Ti₂Fe), their crystal structures are indicated in image (d).

The Ti-Fe eutectoid transformation is reportedly sluggish[29] therefore it was decided that step-quenching samples from a temperature known to homogenise the alloy, to
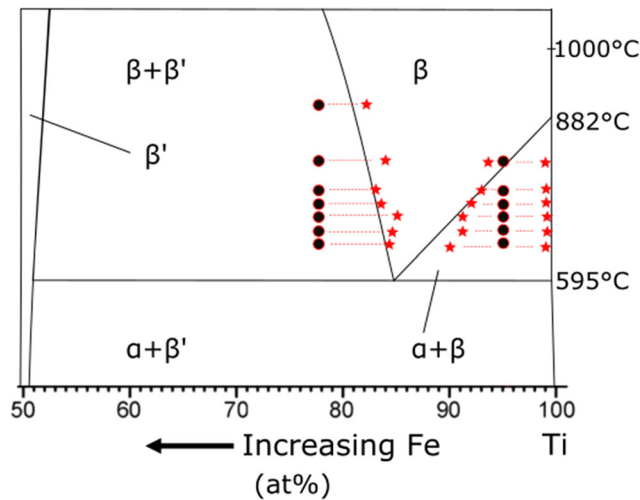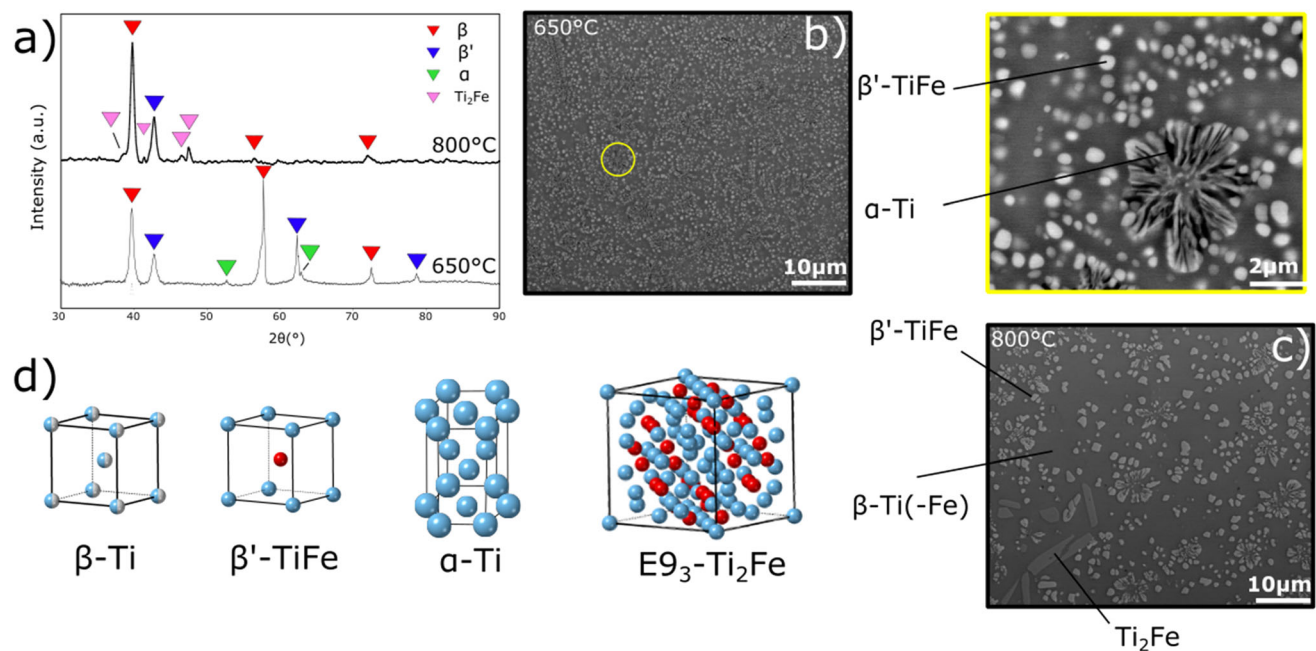

Fig. 3 SEM-EDS results from the β-transus gradient determination in the present work overlaid on the Ti-rich region of the equilibrium Ti-Fe diagram adapted from Murray[16]

Fig. 4 Conventionally aged Ti-22Fe alloy at 650 °C and 800 °C: (a) XRD spectra containing peaks consistent with a 3-phase system at each temperature, (b) BSE image of the microstructure following ageing at 650 °C, the yellow circle highlights the "floret" morphology which is magnified adjacent, (c) BSE image of the microstructure generated following ageing at 800 °C, (d) crystal structures of the phases observed

a temperature purported to be well above the eutectoid temperature of ∼ 600 °C, and isothermally ageing, would permit the precipitation of β′-TiFe only, avoiding any third phase. Figure 5(a) presents a schematic of the heat treatment process, involving a single rapid water quench to avoid heating through the eutectoid. Samples were homogenised at 1050 °C for 24 h and subsequently step-quenched and aged at 650 and 750 °C for specific time periods. The step-quench was achieved by homogenising in a furnace adjacent to a second furnace pre-set to the ageing temperature and then rapidly moving the sample from one to the other.

The spectral profiles of the alloys step-quenched and aged at 650 °C for time periods between 2 and 500 h contain peaks consistently attributable to the β-phase, β′-TiFe phase and the α-Ti phase. A representative XRD spectrum for the alloy aged at 650 °C for 100 h is shown in Fig. 5(b). Calculated a and c parameters of the α-Ti phase were 2.959 Å and 4.689 Å respectively which correlate well to those for pure α-Ti (a = 2.951 and c = 4.684 Å),[16] and did not vary significantly with ageing time. Consistent with conventional heat treatments performed in the determination of the transus gradients, the XRD spectrum for alloys step-quenched and aged at 750 °C for 100 h, shown

in Fig. 5(b), and 500 h (see Appendix Fig. 12) also contained additional peaks attributable to the Ti$_2$Fe phase. The lattice parameters of this non-equilibrium phase are not calculated and are taken to be a = 11.305 Å.[13]

Short duration ageing treatments at 650 °C (up to 4 h) following the step-quench strategy reveal the early stages of the non-equilibrium floret structures, also observed following conventional ageing, nucleate first followed by discrete TiFe precipitates, shown in Fig. 5(c). The presence of the floret morphology suggests the florets nucleate at the ageing temperature and are not a result of heating through the eutectoid region. Following extended isothermal ageing to 100 h and 500 h, the florets realign such that the constituent α-Ti phase adopts a lath morphology (Fig. 5d). The 750 °C step-quench microstructure obtained was of a similar length-scale to that generated by conventional ageing treatments (Fig. 4). Thus, in the Ti-22Fe alloy aged for extended durations, and avoiding heating through the eutectoid, the equilibrium phases at 650 °C were (β + β′ + α) and at 750 °C (β + β′ + Ti$_2$Fe).

By application of distinct heat treatment strategies, several findings become significant: first, the transus gradients and the eutectoid temperature are consistent with previous reports; secondly a three-phase system is obtained
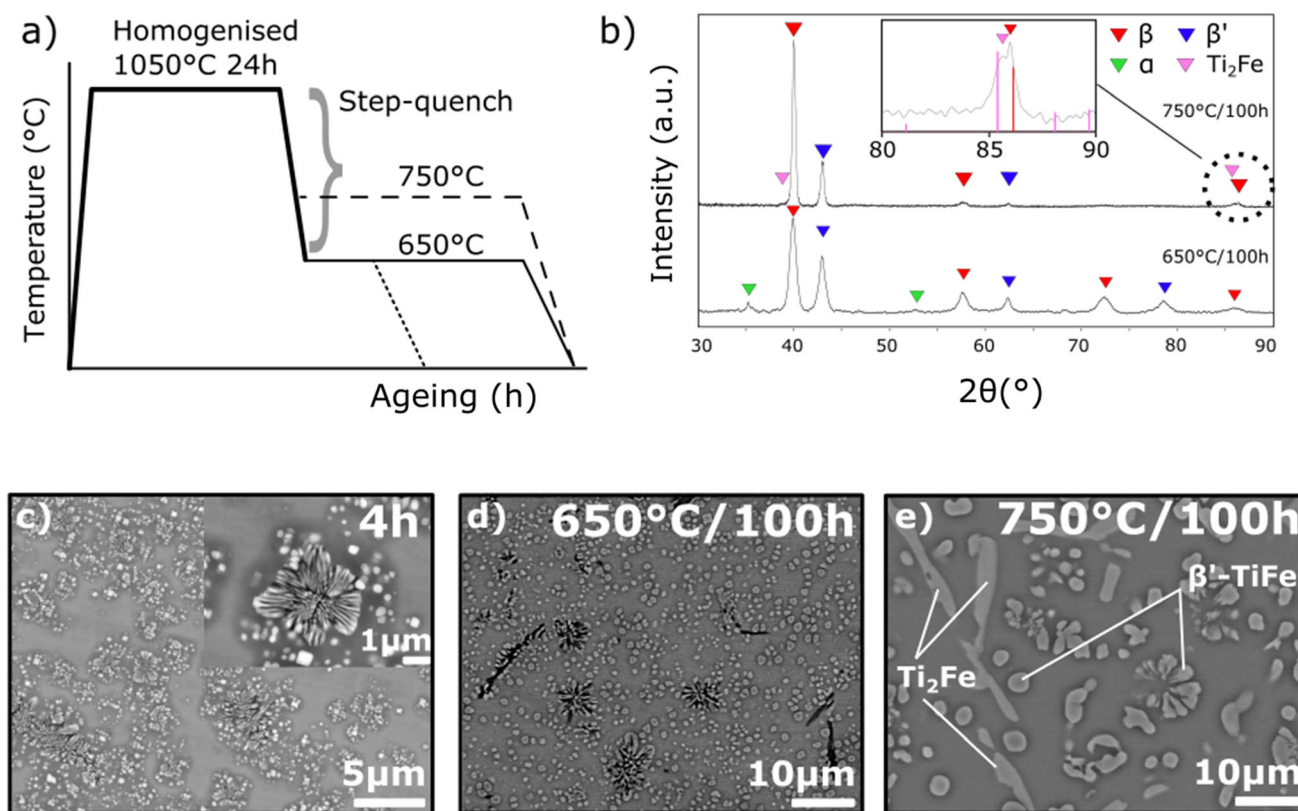

Fig. 5 (a) Step-quench heat treatment methodology employed to bypass the eutectoid, (b) XRD spectra from the aged Ti-22Fe alloy at 650 °C and 750 °C showing the existence of a three-phase system in both conditions, (c) microstructure from the alloy aged at 650 °C for 4 h, and (d) for 100 h, (e) the microstructure following ageing at 750 °C for 100 h

744

J. Phase Equilib. Diffus. (2023) 44:738–750

via both conventional and step-quench methodologies, which removes the contribution of a sluggish eutectoid to the anomalous presence of α-Ti in the anticipated β + β′ dual phase field. Given the affinity of titanium for oxygen, one possibility is that the phase equilibria investigations relate to the ternary Ti-Fe-O system as opposed to the binary Ti-Fe system. As such, chemical analyses have been performed on samples treated by each distinct heat treatment method, the results of which are presented in Table 2. The chemical analyses indicate minor oxygen levels, though an uptake compared to the as-cast results in Table 1 is noted.

Figure 6(a) shows an isothermal section of the Ti-Fe-O system at 650 °C derived from Thermo-Calc TCTI3 database.[28] It is predicted that oxygen additions of just 0.01 at.% are sufficient to enter a three-phase field of (β + β′ + α) for the Ti-22Fe (at.%) alloy under investigation. The experimentally observed phase fraction of the α-Ti phase at 650 °C correlates well to that which is predicted by thermodynamic calculation. Experimentally the α-Ti phase fraction is determined to be 2% by image analyses while the value is predicted to be ⁓1.5% in the Ti-Fe-O system containing 0.1 at.% oxygen. These thermodynamic calculations are summarised in Fig. 6(b) which presents the β-Ti, β′-TiFe and α-Ti phase fractions as a function of temperature for a Ti-22Fe-0.1O alloy. With reference to the impurity levels from Table 2 minor concentrations of oxygen are sufficient to enter the 3-phase field at 650 °C. These oxygen levels are comparable to commercial Ti alloys, and some oxygen will be present in all alloys produced from commercially available titanium sponge. Thus, the experimental assessment of phase equilibria in Ti-X binary systems regarding the stability of α-Ti and Ti₂Fe requires consideration of the influence of oxygen, even when great care is taken to minimise the oxygen content to levels below that found in commercial alloys.

Semiquantitative EPMA analyses of the Ti-22Fe alloy step quenched and aged for 500 h at 650 and 750 °C reveal distinct oxygen enriched regions (no elements other than Ti, Fe and O were detected). Figure 7(a) and (e) present BSE images of the representative microstructures from samples aged at 650 and 750 °C respectively. The dark laths in image (a) are the α-Ti phase, lean in Fe. The coarse laths of light contrast in image (e) are those of the Ti₂Fe

phase. From EPMA elemental mapping of the microstructure at 650 °C, (b–d), it is clearly seen that the regions of oxygen enrichment coincide with the α-Ti laths, while at the higher ageing temperature of 750 °C the enhanced oxygen concentration corresponds to the coarse Ti₂Fe laths (f–h). Thus, since the α-Ti and Ti₂Fe phases are present as a third phase at the respective ageing temperatures, it is reasonable to conclude that they are stabilised by the presence of oxygen.

To investigate the nucleation characteristics and distribution of Fe in the discrete β′-TiFe precipitates, TEM foils were prepared from a location exhibiting the ideal β + β′ microstructure. Figure 8(a) presents a SADP from such a microstructure of an alloy aged for 4 h at 650 °C, with beam parallel to $[001]_\beta$. As expected, β′-TiFe reflections are observed at positions ½$\{200\}_\beta$, highlighted by the red circle in (a), in addition to the primary β-phase reflections. Therefore, a cube-cube orientation relationship exists between these phases, defined as $\{001\}_\beta//\{001\}_{TiFe}$ and $<110>_\beta//<110>_{TiFe}$. The dark field image shown in (b) is generated using the same highlighted superlattice reflection in the selected area diffraction pattern in (a) showing the β′-TiFe precipitates only. STEM-EDS maps and line profile in Fig. 8(c) and (e) confirm the stoichiometry of the discrete β′-TiFe precipitates even after 4h isothermal ageing.

The nature of the α/β relationship in the floret morphology was investigated using conventional TEM and STEM-EDS. STEM-EDS mapping is shown in Fig. 9(a) and (b) for a floret morphology in the Ti-22Fe alloy aged at 650 °C for 100 h, where Fe solute depleted channels (the α-Ti phase) are evident, even after extended ageing. The Burgers orientation relationship between hcp α-Ti and bcc β-Ti phases contains 12 possible variants of α-Ti[29]; 4 variants are shown in a simulated diffraction pattern along $[001]_\beta$ in image (c). Figure 9(d) presents an experimental diffraction pattern along $[001]_\beta$ where intense $\{10\bar{1}1\}_\alpha$ reflections characteristic of the Burgers orientation relation is not present. In addition to primary-β and superlattice β′-TiFe reflections at ½$<200>_\beta$, arced reflections near $\{110\}_\beta$ and $\{200\}$ are present, which do not appear in the Burgers orientation relationship. Close inspection of these arcs, image (e), reveal they are sequential, closely spaced reflections of equal d spacing as opposed to streaks. Additional faint reflections were observed near $\{200\}_\beta$ and one pair are highlighted by the white dashed oval in image (d). Similar diffraction patterns were also observed for ageing durations as short as 1 h at 650 °C (see Appendix). The BF image in Fig. 9(f) shows the same floret as in (a) and (b), where the coloured dashed lines represent outlines of α-Ti variants, summarised from subsequent DF images (Fig. 4g, h, and i). A similar, non-Burgers α/β

Table 2 Impurity level (at.%/ppm) chemical analyses in Ti-22Fe alloys determined by gas fusion method from samples conventionally aged and step quenched

Sample	O	C, ppm	H, ppm	N, ppm
Conv. aged	0.60	63	134	214
Step quench	0.20	824	194	146

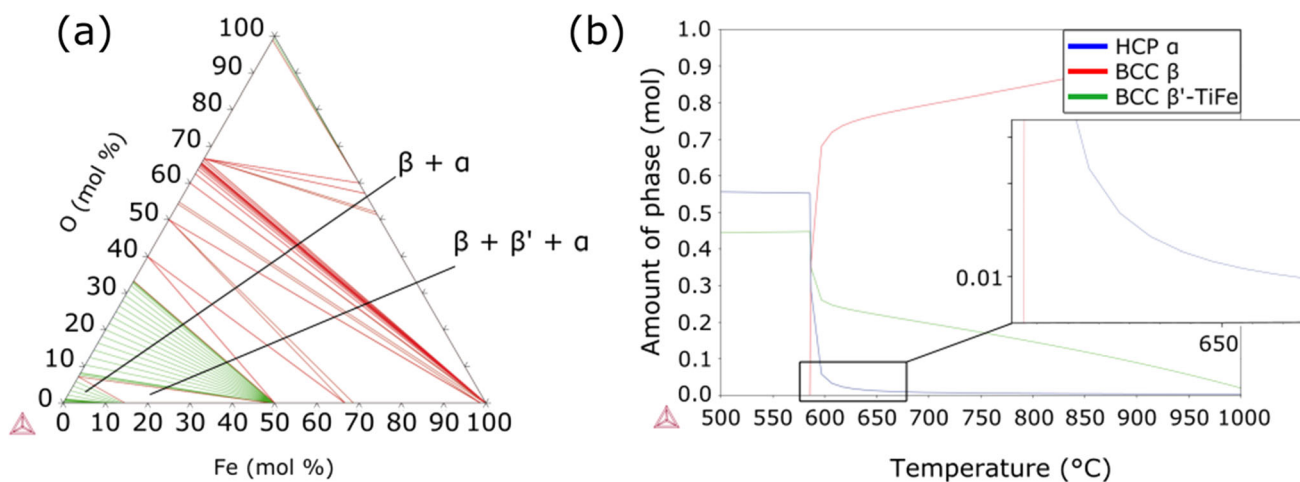J. Phase Equilib. Diffus. (2023) 44:738–750

745

Fig. 6 Ti-Fe-O ternary phase diagrams and phase fractions at 650 °C calculated using Thermo-Calc software[28] and TCTI3 database
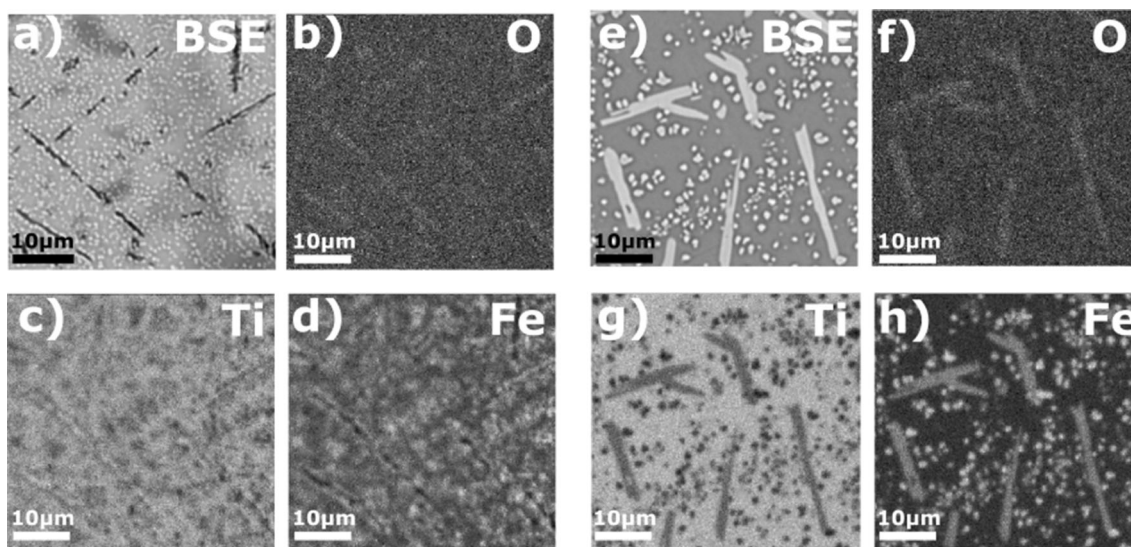

Fig. 7 Ti-22Fe (at%) alloy step quenched and aged for 500 h at 650 °C (a-d) and 750 °C (e-h). BSE-image (a) with β′-TiFe (light region), β-Ti matrix (grey region) and α-Ti (dark region), (b-d) EPMA element maps for O, Ti and Fe clearly illustrating oxygen enriched regions coincident with the α-Ti. The BSE image following ageing at 750 °C (e) with the β′-TiFe and β-matrix as previously, in addition to the coarse Ti$_2$Fe laths (light grey); EPMA elemental maps (f–h) reveal the Ti$_2$Fe laths are enriched by oxygen

relationship has been previously reported in dilute Ti-Mo-Al alloys.[30]

Regarding the floret morphology, it is instructive that the atomic diameters of Ti (1.43 Å) and Fe (1.24 Å) differ by 14% therefore it is plausible that coherency strains make a significant contribution to the total free energy of the alloy. As such, the morphology and, as previously stated, the fact that the floret is the first to nucleate, are suggestive of elastic strain energy considerations. The observed progression of this morphology from short ageing treatments (1, 2, 4 h) reveals that random protrusions form during nascent nucleation while the particles are small—significantly less than 1 μm. There does not appear to be any directional dependency to the growth. At a floret size/diameter of approximately 6 μm, further protrusion growth

ceases and discrete TiFe particles precipitate in the untransformed matrix and at the extremities of the floret.

Based on the microstructural evolution observations, the likely sequence of precipitating phases can be described. In the progression of an isothermal precipitation reaction, the barrier against formation of a new phase, and hence the nucleation rate, is determined by the driving force but also the nucleus/matrix interfacial energy. Therefore, the first nucleating phase will not necessarily be the equilibrium phase with the lowest free energy but that with the lowest nucleation barrier e.g., a metastable phase with a low value of interfacial energy, γ. Such a metastable phase is often an intermetallic compound without the stoichiometry of the equilibrium phase.[31] Once the first nucleating particles have formed, diffusion processes at the precipitate/matrix
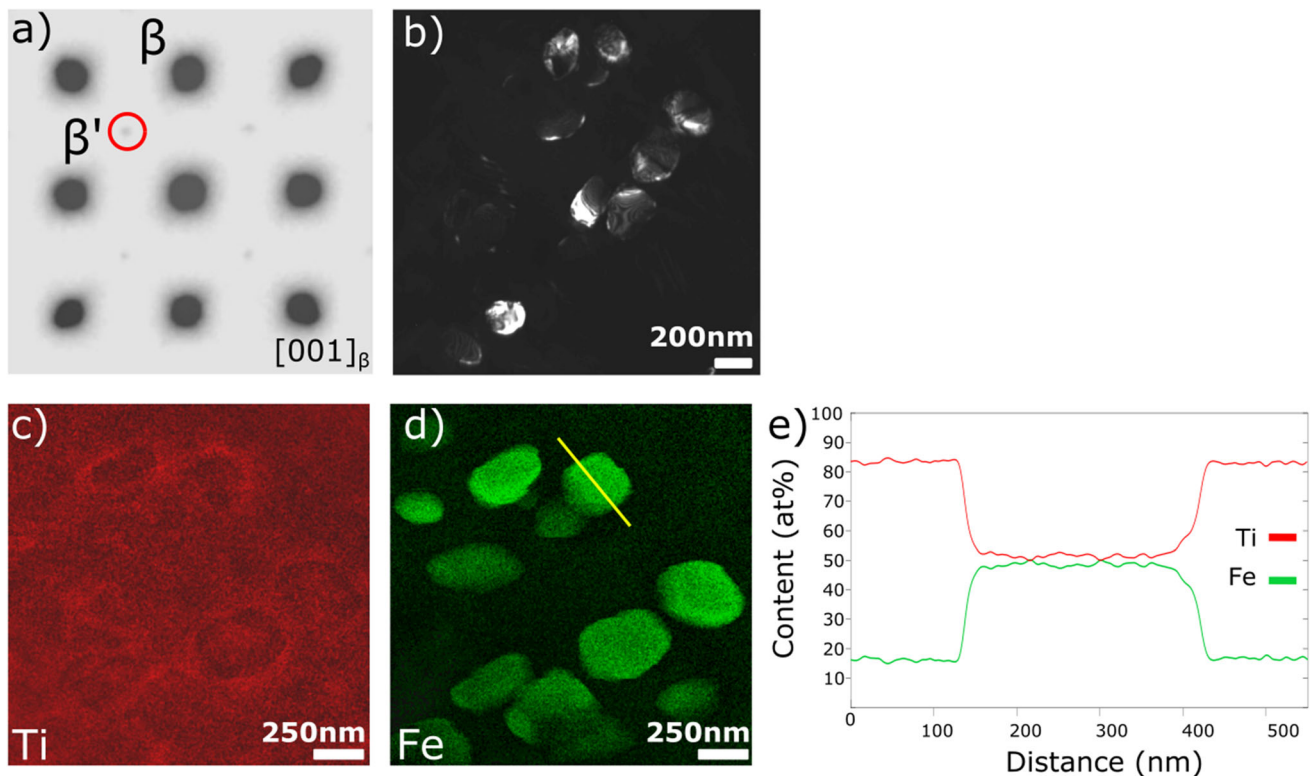
746

J. Phase Equilib. Diffus. (2023) 44:738–750

Fig. 8 Ti-22Fe alloy step quenched to 650 °C and aged for 4 h: (a) TEM diffraction pattern along a [001] zone axis, with $(100)_{TiFe}$ superlattice reflection circled, (b) DF image generated using the same superlattice reflection circled in the diffraction pattern, (c, d) STEM-EDS maps of Ti and Fe, and (e) a composition profile across a discrete β'-TiFe precipitate showing the stoichiometry of this phase.

interface results in the rapid advance of the protrusion into the untransformed β-matrix. It is noteworthy that the diffusion coefficient of Fe in β-Ti is several orders of magnitude greater than the self-diffusion of β-Ti.[32] A simple diffusivity calculation using $2\sqrt{Dt}$ where $D_{Fe} = 1.39 \times 10^{-15}$ m²/s[32] and t = 7200s (= 2 h ageing at 650 °C) gives a diffusion distance of 6 μm which correlates well with the length scale of florets observed following this ageing treatment.

The random manner of the protrusion growth (no directional dependency) suggests isotropy of the matrix and precipitate elastic constants at this early stage.

Further isothermal ageing does not correspond to continuous protrusion growth and discrete TiFe precipitates form. This limit may be interpreted as a threshold in the balance of interfacial energy and elastic strain energy effects. Thus, the nascent stages of the non-equilibrium precipitate growth are likely dominated by interfacial energy effects while the latter stages are dictated by elastic strain energy considerations. Supporting the generality of this precipitation progression, similar nucleation characteristics are also found in nickel superalloys utilising experimental work and phase field modelling to understand unstable γ' precipitate evolution.[33,34]

Extending the ageing time at 650 °C to 500 h, the floret fraction was further reduced compared to 100 h ageing condition, and α-Ti laths were present, as seen in Fig. 5(d). Orientation maps generated by EBSD in Fig. 10(a) indicate that several crystallographic variants of the hexagonal α-Ti are present, each of which has been assigned a different shade dependent upon the crystallographic orientation. The $(0001)_\alpha$ pole figure of these α-variants in addition to the $(011)_\beta$ pole of the parent matrix, Fig. 10(b), are evidence that the orientation relationship between β and lath α phase can be described as:

$$[011]_\beta // [0001]_\alpha; \langle 111 \rangle_\beta // \langle 11\bar{2}0 \rangle_\alpha$$

This relationship between β and α is the Burgers orientation relationship, however it is also clear from the pole figures that some variants do not observe this relationship. This is likely due to incomplete α-phase re-alignment at this stage of ageing but may also be influenced by sample alignment. Thus, between 100 and 500 h the α-Ti constituent of the florets realigns to adopt a lath morphology with a Burgers orientation relation with the β-matrix presumably to sustain low energy interfaces between the two phases and reduce the system strain energy.

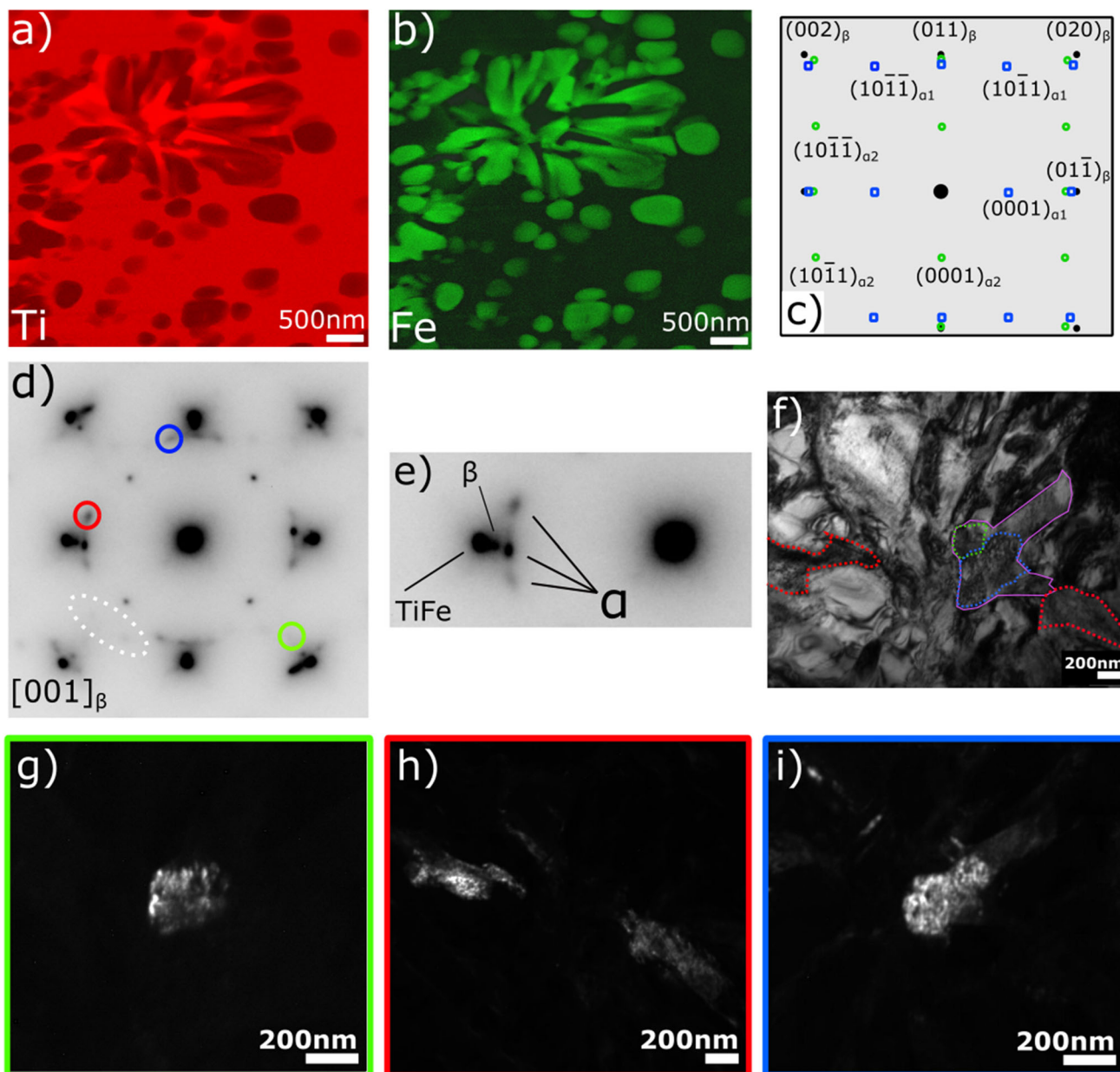By contrast, the coarse Ti₂Fe laths evident following ageing at 750 °C do not reveal any significant texturing,

Fig. 9 α-Ti characteristics in the floret morphology in Ti-22Fe alloy step quenched + aged at 650 °C for 100 h: (a, b) STEM-EDS maps of a typical floret, (c) simulated TEM diffraction pattern aligned along [001]β showing the expected positions of characteristic β-Ti and α-Ti reflections when the Burgers orientation relation is observed, (d) experimental TEM diffraction pattern with beam parallel to [001]β, and magnified view of the $(0\bar{1}1)\beta$ reflection (see text for details), (f) BF image of the floret morphology with beam parallel to [001]β, the colour outlines correspond to DF images (g, i), which are formed by selecting the α-Ti reflections highlighted in the diffraction pattern in (d).

Fig. 10(d). The crystal structure of Ti₂Fe is complex fcc E9₃ (*Strukturbericht* designation), which is also found for intermetallic compounds Ti₂Ni and Ti₂Co.[35] However, unlike the latter compounds, Ti₂Fe does not share the a $(011)_\beta//(011)_{Ti_2Fe}$, $[111]_\beta//[11\text{-}1]_{Ti_2Fe}$ orientation relation.

Table 3 presents a summary of the measured composition and lattice parameters of each phase observed following step quench and ageing heat treatments at 650 and 750 °C for 500 h. Compositions were measured by SEM-EDS and STEM-EDS as indicated. It is important to note that the EDS results are semi-quantitative, given the contribution from beam spreading, interaction volume and spatial resolution of the EDS detector.

748

J. Phase Equilib. Diffus. (2023) 44:738–750

Fig. 10 Ti-22Fe alloy step quenched—aged (a) at 650 °C for 500 h showing EBSD orientation map for α-Ti and (b) in the same heat treatment condition, the pole figures showing $(0001)_\alpha$ and $(011)_\beta$ where particular α-and β-poles lie parallel, (c) step quenched -aged at 750 °C for 500 h showing EBSD orientation map for the Ti$_2$Fe phase and (d) the same heat treatment condition showing pole figures for $(111)_{Ti2Fe}$ and $(011)_\beta$ where a single Ti$_2$Fe pole lies parallel to a β-pole
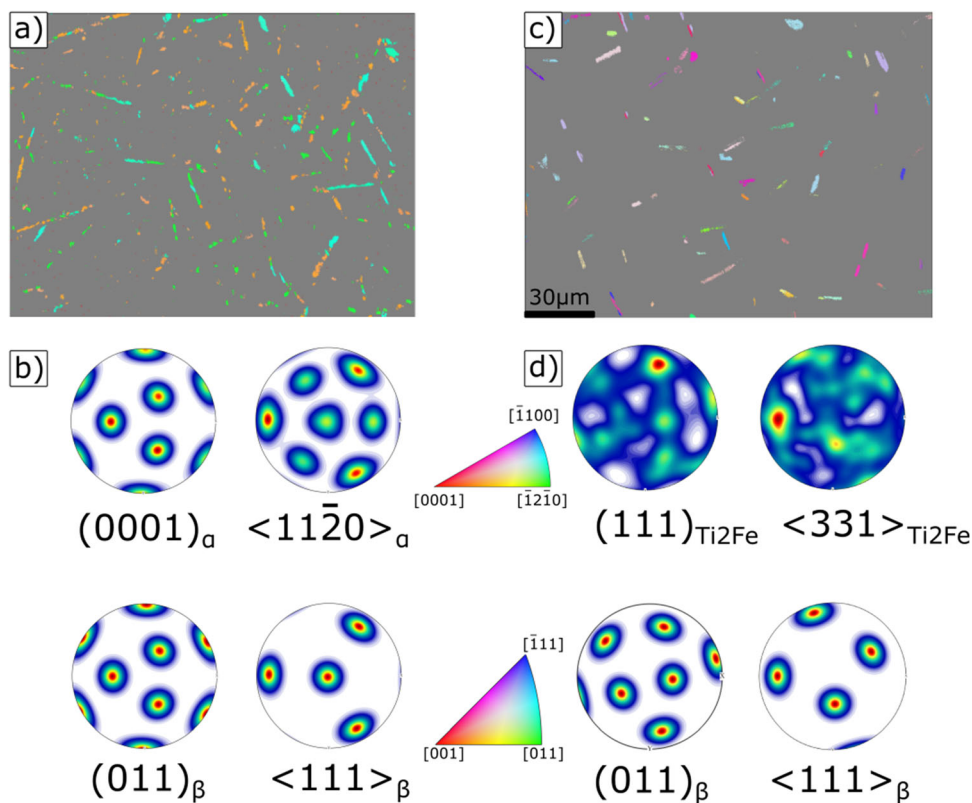
Table 3 Compositions and lattice parameters of each phase observed at 650 °C and 750 °C measured by SEM-EDS, STEM-EDS and XRD

Heat treatment	Phase A (A2)		Phase B (B2)		Phase C (A3)		Phase D (Ti₂Fe)	
	Composition (Fe at.%)	Lattice param, nm	Composition (Fe at.%)	Lattice param (nm)	Composition (Fe at.%)	Lattice param, nm	Composition (Fe at.%)	Lattice param, nm
650/500h	16.7 ± 1.2	0.319	53.2 ± 2.3	0.298	*1.9 ± 2.4	a: 0.296 c: 0.475		
750/500h	14.9 ± 0.2	0.319	45.2 ± 0.7	0.298			30.8 ± 3.1	1.126**

*STEM-EDS measurements
**Ref. [13]

3 Conclusions

The initial design intent of this work was to produce and evaluate dual phase β + β′ microstructures by ageing a Ti-22Fe alloy in the supposed two-phase field. However, it has not been possible to obtain such microstructures even when bypassing the sluggish eutectoid, with three-phase microstructures instead found. The β-transus gradients have been evaluated and are accurate, as is the eutectoid temperature.

Step-quenching to an ageing temperature of 650 °C results in a 3-phase system consisting of β-Ti + β′-TiFe + α-Ti. Step-quenching and ageing at 750 °C also produces a three-phase system of β-Ti + β′-TiFe + Ti$_2$Fe. At each temperature, the third phase appears to be stabilised by the presence of oxygen, even at contents ∼ 1500 ppm O, which are typical of commercial Ti alloys. Thermodynamic predictions indicate oxygen contents of 0.01 at.% to Ti-22Fe are sufficient to stabilise a three-phase field of β-Ti + β′-TiFe + α-Ti at 650 °C.

This work indicates that the modelling and stability of α-Ti and Ti$_2$Fe with alloying additions are important considerations to avoid their formation in the onward development of β-Ti bcc-superalloys reinforced by β′-TiFe precipitates.
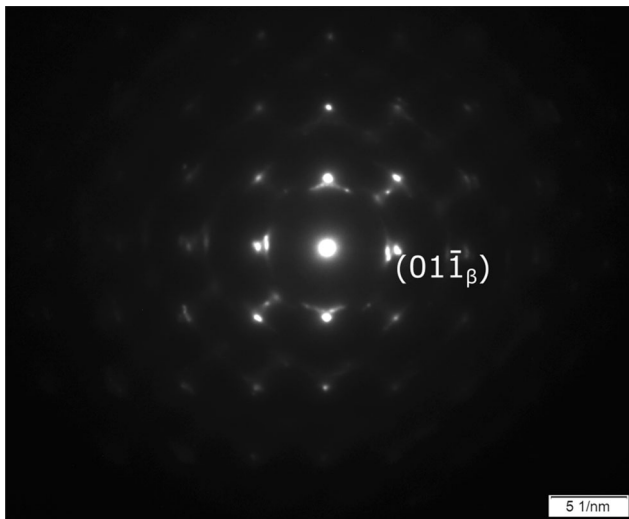
Appendix

See Figs. 11 and 12.

J. Phase Equilib. Diffus. (2023) 44:738–750

749

Fig. 11 Diffraction pattern of Ti-22Fe alloy aged for 1 h at 650 °C
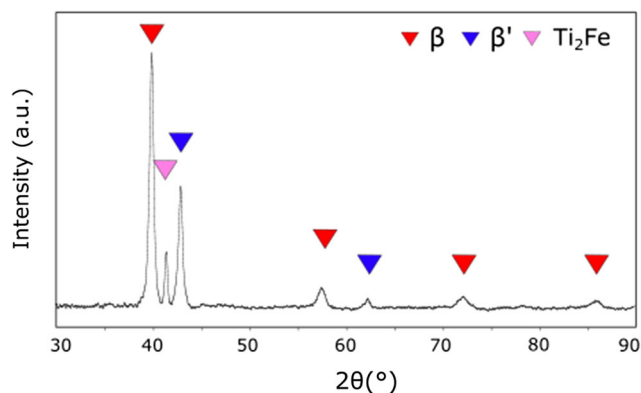
Fig. 12 XRD spectrum of Ti-22Fe alloy that was step-quenched and aged at 750 °C for 500 h

References

1. S. Naka, and T. Khan, Designing Novel Multiconstituent Inter-metallics: Contribution of Modern Alloy Theory in Developing Engineered Materials, *J. Phase Equilib. Diffus.*, 1997, **18**(6), p 635-649.

2. G. Ghosh, and G.B. Olson, Integrated Design of Nb-Based Superalloys: Ab initio Calculations, Computational Thermody-namics and Kinetics, and Experimental Results, *Acta Mater.*, 2007, **55**, p 3281-3303.

3. J. Peng, S. Li, Y. Mao, and X. Sun, Phase Transformation and Microstructures in Ti-Al-Nb-Ta System, *Mater. Lett.*, 2002, **53**, p 57-62.

4. P. Alonso, P. Gargano, P. Bozzano, G. Ramirez-Cabellero, P. Balbuena, and G. Rubiolo, Combined ab initio and Experimental Study of A2+L2$_1$ Coherent Equilibria in the Fe-Al-X (X = Ti, Nb, V) Systems, *Intermetallics*, 2011, **19**, p 1157-1167.

5. S. Emura, K. Tsuzaki, and K. Tsuchiya, Improvement of Room Temperature Ductility for Mo and Fe Modified Ti$_2$AlNb Alloy, *Mater. Sci. Eng. A*, 2010, **528**, p 355-362.

6. A.J. Knowles, D. Dye, R.J. Dodds, A. Watson, C.D. Hardie, and S.A. Humphy-Baker, Tungsten-Based bcc-Superalloys, *Appl. Mater. Today*, 2021, **23**, 101014.

7. R.D. Jones, A.J. Knowles, and W.J. Clegg, A Binary β Titanium Superalloy Hardened by TiFe Precipitation, α and ω, *Scr. Mater.*, 2021, **200**, 113905.

8. H. Donthula, B. Vishwanadh, T. Alam, T. Borkar, R. Contieri, R. Caram, R. Banerjee, R. Tewari, G. Dey, and S. Banerjee, Mor-phological Evolution of Transformation Products and Eutectoid Transformation(s) in a Hyper-Eutectoid Ti-12 at% Cu Alloy, *Acta Mater.*, 2019, **168**, p 63-75.

9. A. Devaraj, S. Nag, R. Srinivasan, R.E.A. Williams, S. Banerjee, R. Banerjee, and H.L. Fraser, Experimental Evidence of Con-current Compositional and Structural Instabilities Leading to W Precipitation In Titanium-Molybdenum Alloys, *Acta Mater.*, 2012, **60**, p 596-609.

10. J.J. Reilly, and R.H. Wiswall, Formation and Properties of Iron Titanium Hydride, *Inorg. Chem.*, 1974, **13**(1), p 218-222.

11. T.B. Massalski, *Binary Alloy Phase Diagrams*, Vol. 2, 2nd edn. ASM International, Detroit, 1990, p1783

12. R.J. VanThyne, H.D. Kessler, and M. Hansen, The Systems Titanium-Chromium and Titanium-Iron, *Trans. Am. Soc. Met.*, 1953, **44**, p 974-989.

13. D.H. Polonis, and J.G. Parr, Phase Transformations in Titanium-Rich Alloys of Iron and Titanium, *Trans. Am. Inst. Min. Met. Eng.*, 1954, **200**, p 1148-1154.

14. P. Duwez, and J. Taylor, The Structure of Intermediate Phases in Alloys of Titanium with Iron, Cobalt and Nickel, *Trans. AIME*, 1950, **188**, p 1173-1176.

15. E. Ence, and H. Margolin, Re-examination of Ti-Fe and Ti-Fe-O Phase Relations, *Trans. Am. Inst. Min. Met. Eng.*, 1956, **206**, p 572-577.

16. J.L. Murray, The Fe-Ti System, *Bull. Alloy Phase Diagr.*, 1981, **2**, p 320-334.

17. A. Salmasi, S.J. Graham, I. Galbraith, A.D. Graves, M. Jackson, S. Norgren, D. Guan, H. Larsson, and L. Höglund, Mobilities of Ti and Fe in Disordered TiFe-BCC Assessed from New Experi-mental Data, *Calphad*, 2021, **74**, 102300.

18. L. Kaufmann, and H. Nesor, Coupled Phase Diagrams and Thermochemical Data for Transition Metal Binary Systems—1, *Calphad*, 1978, **2**(1), p 55-80.

19. L.F.S. Dumitrescu, and M. Hillert, Comparison of Fe-Ti Assessments, *J. Phase Equilib.*, 1998, **19**(5), p 441-448.

750

J. Phase Equilib. Diffus. (2023) 44:738–750

20. K.C. Hari Kumar, P. Wollants, and L. Delaey, Thermodynamic Reassessment and Calculation of Fe-Ti Phase Diagram, *Calphad*, 1994, **18**(2), p 223-234.

21. S. Jonsson, Assessment of the Fe-Ti System, *Metall. Mater. Trans. B*, 1998, **29B**, p 361-385.

22. H. Ohtani, N. Hanaya, M. Hasebe, S. Teraoka, and M. Abe, Thermodynamic Analysis of the Fe-Ti-P Ternary System by Incorporating First-Principles Calculations into the CALPHAD Approach, *Calphad*, 2005, **30**, p 147-158.

23. R. Ray, B.C. Giessen, and N.J. Grant, The Constitution of Metastable Titanium Rich Ti-Fe Alloys: An Order-Disorder Transition, *Metall. Trans.*, 1972, **3**, p 627-629.

24. D. Dew-Hughes, The Addition of Mn and Al to the Hydriding Compound FeTi: Range of Homogeneity and Lattice Parameters, *Metall. Trans. A*, 1980, **11**, p 1219-1225.

25. S. Wang, K. Wang, G. Chen, Z. Li, Z. Qin, X. Lu, and C. Li, Thermodynamic Modelling of Ti-Fe-Cr Ternary System, *Calphad*, 2017, **56**, p 160-168.

26. C. Guo, C. Li, X. Zheng, and Z. Du, Thermodynamic Modelling of the Fe-Ti-V System, *Calphad*, 2012, **38**, p 155-160.

27. J.B. Nelson, and D.P. Riley, An Experimental Investigation of Extrapolation Methods in the Derivation of Accurate Unit Cell Dimensions of Crystals, *Proc. Phys. Soc.*, 1945, **57**, p 160-177.

28. H. Lukas, S.G. Fries, and B. Sundman, *Computational Thermodynamics: The CALPHAD Method*. Cambridge University Press, Cambridge, UK, 2007.

29. G. Lutjering, and J.C. Williams, *Titanium*, 2nd edn. Springer, Berlin, 2007.

30. C.G. Rhodes, and J.C. Williams, The Precipitation of α-Phase in Metastable β-Phase Ti Alloys, *Met. Trans. A*, 1975, **6A**, p 2103-2114.

31. R. Wagner, R. Kampmann, and P.W. Voorhees, Homogeneous second phase precipitation, in *Phase Transformations in Materials*. G. Kostorz, Ed., Wiley, Weinheim, 2001, p309-407

32. H. Mehrer, *Diffusion in Solid Metals and Alloys*, Vol. 26. Springer, Berlin, 1990.

33. R.A. Ricks, A.J. Porter, and R.C. Ecob, The Growth of γ' Precipitates in Nickel-Base Superalloys, *Acta Metall.*, 1983, **31**, p 43-53.

34. N. Krutz, C. Shen, M. Karadge, A. J. Egan, J. R. Bennett, T. Hanlon, and M. J. Mills, An approach toward understanding unstable gamma prime precipitate evolution and its effect on properties, superalloys 2020, in *Proceedings of the 14th International Symposium on Superalloys, TMS*, 2020, p 691-701.

35. W. Rostoker, Observations on the Occurrence of Ti2X Phases, *JOM*, 1952, **4**(2), p 209-210.